DOI: 10.1021/ma100464z

Macromolecules
ARTICLE

Hydrogels from ABA and ABC Triblock Polymers

Rajiv R. Taribagil,[†] Marc A. Hillmyer,*[,‡] and Timothy P. Lodge*[,†,‡]

[†]*Department of Chemical Engineering & Materials Science and* [‡]*Department of Chemistry, University of Minnesota, Minneapolis, Minnesota 55455-0431*

Received February 27, 2010; Revised Manuscript Received May 3, 2010

ABSTRACT: Aqueous gels of telechelic poly(ethylene oxide) (PEO)-based triblock polymers, with homo and hetero combinations of 1,2-polybutadiene (PB) and poly(perfluoropropylene oxide) (PFPO) as hydrophobic end-blocks, were prepared by anionic polymerization and polymer−polymer coupling reactions. The block molecular weights in kg/mol were (2.7−24−2.7) for PB-*b*-PEO-*b*-PB, (2.3−23−2.3) for PFPO-*b*-PEO-*b*-PFPO, and (1.9−26−2.3) for PB-*b*-PEO-*b*-PFPO. Gels with polymer concentrations ranging from 10 to 50 wt % were investigated using cryogenic scanning electron microscopy (cryo-SEM) and small-angle neutron scattering (SANS). The cryo-SEM micrographs revealed significant differences among the morphologies of the gels obtained, depending on the end-blocks used. Results from contrast matching SANS experiments were used to corroborate and refine the information obtained from microscopy. The PB-*b*-PEO-*b*-PB copolymers formed networks of spherical micelles at all concentrations as expected, albeit with significant spatial heterogeneity that diminished with increasing concentration. The PFPO-*b*-PEO-*b*-PFPO copolymers also formed networks by aggregation of the end-blocks, but the PFPO blocks tended to adopt disklike or even sheetlike structures. This is attributed to the extremely high interfacial tension of PFPO with water and is consistent with the "super-strong" segregation regime behavior. The heterotelechelic PB-*b*-PEO-*b*-PFPO terpolymers adopted a quite different structure, namely an intricate bicontinuous open-cell foam, with cells on the order of 500 nm in size and cell walls composed of PFPO disks embedded in PB sheets. These various network structures illustrate the potential of using end-block chemistry to manipulate both the morphology and the physical properties of polymer gels.

Aqueous dispersions of triblock polymers with soluble mid-blocks have received widespread attention, due in part to their ability to range from viscous liquids to elastic solids, thereby enabling a host of applications in the fields of coatings, cosmetics, pharmaceutics, and oil recovery. Flow modification stems from the chain architecture−long hydrophilic mid-blocks with short hydrophobic end-blocks−and the physical association of the end-blocks.[1] Upon hydration at low copolymer concentrations, the hydrophobic blocks associate to form micellar cores with the hydrophilic block looping or back-folding into the same core. With an increase in concentration and the resulting increase in the number density of these micelles, the mid-block can overcome the entropic penalty of back-folding by bridging to another micellar core.[2] With more bridging, the viscosity of the solution starts to rise steeply, solidlike behavior emerges, and a gel is formed.[3,4]

Early experiments with dilute aqueous solutions of telechelic poly(ethylene oxide) (PEO) with small paraffinic end-caps indicated that the size and type of end-groups dictated their morphological behavior. For smaller hydrophobes, the enthalpic penalty of exposing them to water outweighs the entropic penalty of mid-block looping, and the polymers form loose open aggregates.[5,6] Substituting paraffinic groups with longer polymeric blocks or with more water-averse groups like fluorocarbons yields compact micellar structures, wherein the mid-block ends are confined to a common core.[7−13] As concentration is increased, micellar bridging leads to gelation.[14] With further increase in concentration, such systems often display a sequence of ordered (liquid crystalline) phases.[15−17] Of particular relevance to the work reported here, Agrawal et al. investigated polylactide-*b*-PEO-*b*-polylactide triblocks in water and found a strong dependence of association behavior on the tacticity of the polylactide block;[18] atactic polylactide blocks form amorphous spherical domains, which associate in an isotropic manner to form a network, isotactic polylactide blocks form crystalline disklike domains, and association proceeds by stacking of disks. Tae et al. found that mixtures of fluorocarbon telechelics and water exhibit ordering transitions to cubic phases with increase in concentration.[19] They also concluded that the chemical nature of the hydrophobe plays an important role in determining the structure as well as the association behavior of the micelle. Fluoroalkyl groups were believed to behave as short rods laterally constraining the PEO chains, whereas alkyl groups formed liquidlike spherical cores.[20] This dissimilarity in the assembly of hydrophobic groups has been attributed to the difference in the interfacial tension that these groups exhibit with the water−PEO environment. Further comparative investigations into the association behaviors of telechelic polymers with fluoropolymers and their hydrocarbon equivalents as termini are warranted and constitute a basis for studying compartmentalized hydrogels, i.e., aqueous polymeric networks with two or more chemically distinct hydrophobic domains.

Development of assemblies such as micelles and gels with distinguishable multiple subdomains or compartments is aimed at mimicking the structural intricacy of biological entities such as proteins, organelles, and cells, which possess subdomains on the nanometer scale that enable them to perform multiple functions simultaneously. Several groups have succeeded in preparing multicompartment micelles in water or in water−organic solvent mixtures, where incompatible hydrophobic polymers microphase segregate into separate domains in the micellar core.[21−42] In the case of multicompartment networks, Weberskirch et al. studied

*Authors for correspondence. E-mail: hillmyer@umn.edu (M.A.H.), lodge@umn.edu (T.P.L.).

 Published on Web 05/28/2010

segregation of end groups in a concentrated (~30 wt % polymer) aqueous dispersion of telechelic poly(2-methyl-2-oxazoline), with *n*-alkyl and *n*-perfluoroalkyl moieties at the termini, using NMR spectroscopy. Although the end groups formed separate domains, the morphology of the domains was not resolved.[43] Similarly, Shunmugam et al. showed that polyacrylate-based ABC triblocks, with hydrophilic and fluorophilic end-groups, formed hydrogels,[44] but no morphological characterization was reported. Shen et al. demonstrated that in hydrogels formed from artificial proteins with dissimilar end-domains the incompatible end-groups suppress looping of the mid-block, and they tend not to associate with each other.[45]

While exclusive bridging of mid-blocks might be naïvely expected for any ABC terpolymer network with immiscible A and C blocks, the interplay of the interactions among the three blocks and the solvent can offset the significance of incompatibility between the end-blocks and give rise to different microstructures. Recently, we communicated a representative example of such an interplay in water containing 10 wt % of a linear terpolymer of 1,2-polybutadiene (PB), poly(ethylene oxide) (PEO), and poly(perfluoropropylene oxide) (PFPO); a telechelic architecture with a long hydrophilic block (PEO) end-capped with mutually incompatible hydrophobic blocks (PB and PFPO).[46] Rather than adopting a two-compartment network with spatially distinct PB and PFPO micelles, the terpolymer assembled into a percolating, foamlike structure, as revealed by cryogenic scanning electron microscopy (cryo-SEM). Contrast-matching small-angle neutron scattering (SANS) analysis was used to establish the presence of a structural motif in which the PFPO blocks assemble into disks and are embedded in thin bicontinuous PB sheets with both faces of the sheets covered by looped PEO brushes. In this article, we show that the bicontinuous arrangement of the two hydrophobic blocks, previously reported for a single concentration, is consistently observed over a wide range of concentration. Furthermore, we present a detailed comparative study on the structural and association behavior of telechelic PEO with homo- and heterocombinations of the same hydrophobic blocks (PB and PFPO).

Materials and Methods

Materials. We prepared three types of telechelic PEO triblocks: two homo combinations and one hetero combination, with PB and PFPO as end-blocks (Figure 1). These molecules are henceforth designated BOB, FOF, and BOF, respectively. 1,2-Polybutadiene-*b*-poly(ethylene oxide) (PB−PEO) diblock copolymers were synthesized using two successive living anionic polymerizations.[47] To obtain BOB, the living chains were coupled with slow addition of a stoichiometric amount of α,α′-dibromo-*p*-xylene.[48] In case of BOF, the reaction was terminated by addition of acidic methanol, thereby yielding a hydroxyl-terminated diblock copolymer. Commercially available carboxylic acid end-capped PFPO was converted to the acid chloride derivative by reacting with oxalyl chloride. The final BOF terpolymer was obtained by coupling the hydroxy end-functional PB−PEO with the acid chloride end-functional PFPO.[46] FOF was synthesized by reacting α,ω-dihydroxy-PEO, obtained from Sigma-Aldrich, with acid chloride end-functional PFPO. The molecular weights and polydispersity indices of each block were determined using NMR spectroscopy and size exclusion chromatography (with polystyrene standards), respectively; the detailed results are included in the Supporting Information. Table 1 summarizes the molecular characteristics of the three triblock polymers.

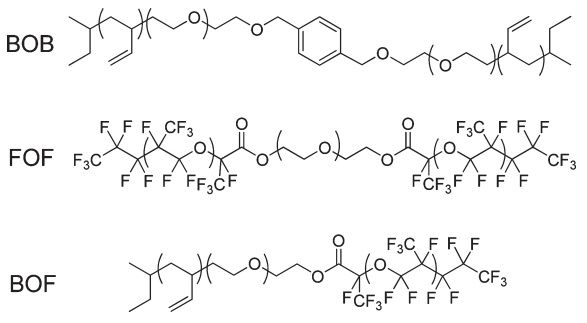

Figure 1. Chemical structures of the three triblock polymers used in this study.

Sample Preparation. The desired mass of polymer was dissolved in a vial containing dichloromethane. The solution was allowed to dry overnight under a flow of N_2 so as to leave a thin film of polymer at the bottom of the vial. To ensure complete removal of dichloromethane, the polymer film was dried under vacuum at RT for 2 days. The film was then hydrated with a defined amount of water and stirred at 65 °C for 24 h. The solution was then cooled and held at RT with moderate stirring for at least 1 week prior to subsequent characterization. Water (H_2O, Chromasolv grade) was used as solvent for cryogenic scanning electron microscopy (cryo-SEM) experiments. For small-angle neutron scattering (SANS) experiments, mixtures of water and heavy water (D_2O, 99.9% D, Cambridge Isotopes), with compositions varying according to the polymer block to contrast match, were used as solvents.

Cryogenic Scanning Electron Microscopy (Cryo-SEM). Cryo-SEM experiments were conducted on 10 and 30 wt % polymer dispersions following the protocol described in our recent publication.[46] A small amount of the sample was sandwiched between two "freezing hats" each about 100 μm deep, taking care to exclude air. Using a Bal-Tec HPM 010 high-pressure freezing machine (Balzers, Lichtenstein, operating pressure of 2100 bar), the assembly was rapidly cooled. The cooled assembly was then moved into a liquid nitrogen bath and pried open with a scalpel to fracture the sample, exposing its interior. Vitrified water near the surface and a few micrometers deep into the sample was then partially sublimed in a Balzers MED 010 freeze-drying and sputtering device at −96 °C and ~2×10^{-9} bar for about 5 min. The exposed surface was then coated with an 8 nm thick conducting layer of platinum at −130 °C. The coated sample was transferred at −150 °C into a Hitachi S900 in-the-lens field emission scanning electron microscope, maintained at about −170 °C, and examined at a low acceleration voltage of 2 keV to avoid excessive charging and radiation damage of the areas imaged. The procedure described above yields samples with few artifacts arising from freezing and high topographical contrast as the polymeric framework is resolved relative to voids (previously water-filled chambers), which are formed as the vitrified water sublimes.[49]

Table 1. Molecular Parameters of Linear Triblock Copolymers

sample ID	total N_{PB}[a]	N_{PEO}[a,b]	total N_{PFPO}[c]	f_{PB}[d]	f_{PEO}[d]	f_{PFPO}[d]	M_n[e] (kg/mol)	PDI[f]
BOB	100	591[a]		0.21	0.79		31.4	1.11
BOF	38	596[a]	12	0.08	0.87	0.05	30.2	1.08
FOF		522[b]	24		0.89	0.11	27.6	1.07

[a] Calculated using ^{1}H NMR spectroscopy. [b] Calculated using SEC with light scattering detection. [c] Calculated using ^{19}F NMR spectroscopy. [d] The volume fractions were calculated using the molecular weight and the RT densities of ρ(PB) = 0.89 g/cm^3, ρ(PEO) = 1.12 g/cm^3 (amorphous), and ρ(PFPO) = 1.9 g/cm^3. [e] The total molecular weight of each triblock polymer was calculated from the NMR spectra and SEC with light scattering detection. [f] The PDI was determined by SEC using PS standards and THF as solvent at 40 °C.

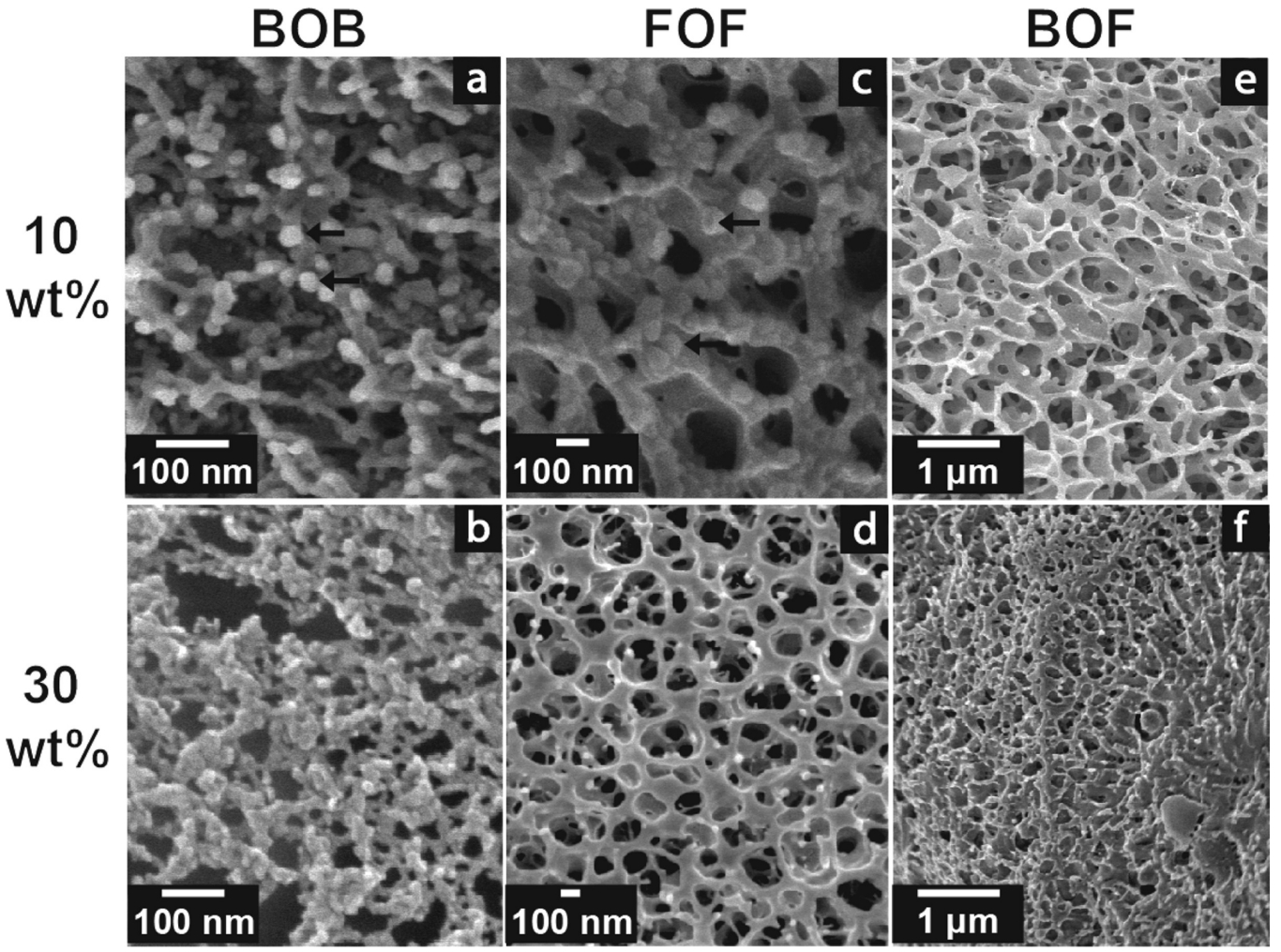

Figure 2. Cryo-SEM micrographs of aqueous solutions of (a) 10 wt % BOB, (b) 30 wt % BOB, (c) 10 wt % FOF, (d) 30 wt % FOF, (e) 10 wt % BOF, and (f) 30 wt % BOF. Arrows in (a) and (c) indicate spheres and flatter disklike entities, respectively.

Small-Angle Neutron Scattering (SANS). SANS experiments were conducted on aqueous samples with polymer concentrations of 10, 20, 30, 40, and 50 wt % at 25 °C. Contrast matching was used in tandem with scattering to gain detailed information about individual components in multicomponent mixtures.[46] Briefly, contrast matching involves choosing a solvent environment with scattering length density (ρ^*) equal to that of the component to be contrast matched. For aqueous systems, this is done by mixing water ($\rho^* = -5.6 \times 10^9$ cm^{-2}) and heavy water ($\rho^* = 6.38 \times 10^{10}$ cm^{-2}). Solutions of BOB were prepared in D_2O, as the scattering length densities of PB ($\rho^* = 4.11 \times 10^9$ cm^{-2}) and PEO ($\rho^* = 6.38 \times 10^9$ cm^{-2}) are very close in magnitude. FOF was dispersed in a PEO contrast matched mixture. In the case of BOF, samples were prepared under two different contrast-match conditions for each concentration, namely PEO matched and PFPO ($\rho^* = 4.11 \times 10^{10}$ cm^{-2}) matched. Samples were sandwiched between two quartz disks separated by a 1.5 mm aluminum spacer. The scattering experiments were performed at the National Institute of Standards and Technology (NIST) on the NG-7 30 m instrument of the Cold Neutron Research Facility.[50] As we have described previously,[46] sample-to-detector distances of 1 and 11 m with a monochromated neutron wavelength (λ) of 7 Å and a wavelength spread ($\Delta\lambda/\lambda$) of 0.11 were used to cover scattering wave vectors from 0.0036 to 0.37 Å^{-1}. Using Igor Pro Macros, the resulting data were corrected for background, nonuniform detector efficiency, solvent (scattering contribution weighted by its volume fraction in the solution)[51] plus empty cell scattering, and sample transmission.[52] The scattering intensities were then scaled to absolute values on the basis of direct beam flux measurements. For FOF and BOF samples, the incoherent background was estimated from the asymptotic slope of a Porod plot (Iq^4 vs q^4) and subtracted before data evaluation.

Results

Representative cryo-SEM images from each of the six samples examined are shown in Figure 2. Clear differences in structure appear among the three polymers and also between 10% and 30% solutions for FOF. The BOB images are consistent with networks of spherical micelles, with a significant number of voids larger than 100 nm. The FOF 10% solution presents a network of disklike micelles, also with large voids, whereas the 30% solution resembles an open cell foam. The BOF structure is also foamlike at both concentrations, but note that the scale is almost an order of magnitude larger than for BOB and FOF. We now consider these structures in more detail, including analysis of the SANS profiles.

The 10 and 30 wt % BOB samples showed clusters of spheres with diameters in the range of 25−30 nm (Figure 2a,b). This dimension includes the ca. 8 nm thick Pt coat and presumably some contribution from the PEO chains. Considering that PEO accounts for about 80% of the total triblock molecular volume, we estimate the radius of the underlying hydrophobic core to be between 5 and 10 nm. The SANS intensity profiles of the BOB

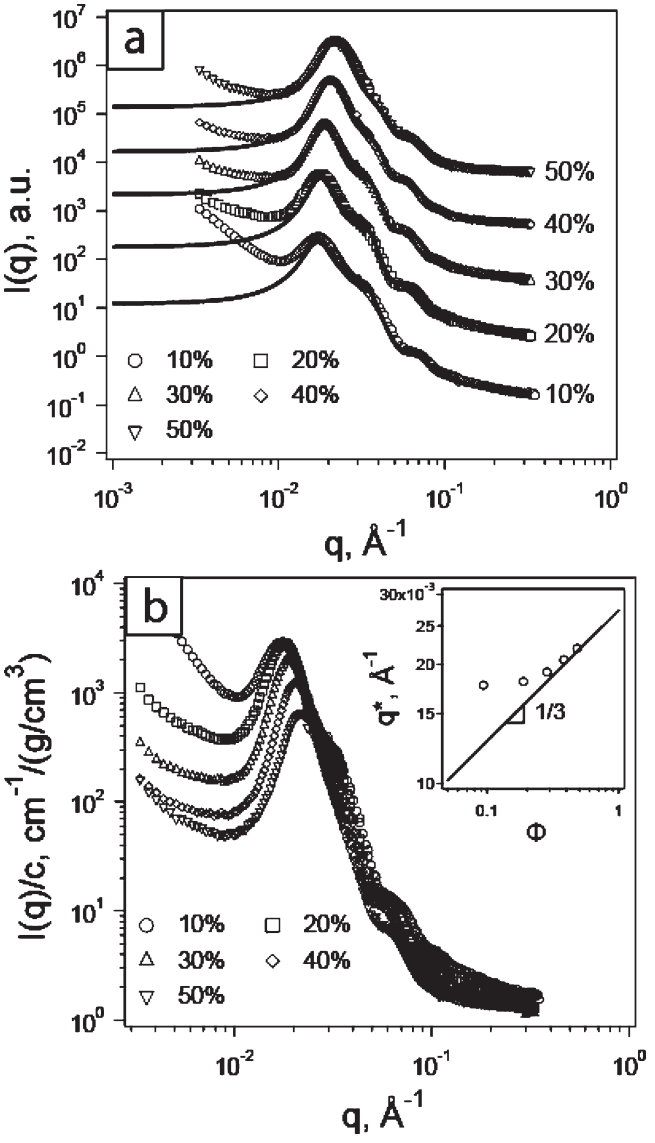

Figure 3. (a) SANS intensity profiles for BOB at different concentrations in water, with both PB and PEO contributing to scattering. For clarity, the intensity data for higher concentrations have been shifted vertically: 20% (×10), 30% (×100), 40% (×1000), 50% (×10000). The solid lines are fits using eqs A2−A8. (b) Intensity profiles normalized by concentration. Inset shows the dependence of peak position on polymer volume fraction.

samples with polymer concentrations ranging from 10 to 50 wt % are shown in Figure 3a. The upturn in intensity at low q is consistent with the large voids (water-filled chambers prior to sublimation) revealed in the cryo-SEM. Furthermore, on normalizing the intensity data by the concentrations of BOB, all the profiles show similar q dependences (Figure 3b), demonstrating the invariance of shape and dimensions of the hydrophobic domains with respect to changes in concentration. Variations in the unsubtracted backgrounds account for the small lack of overlap in the high q region. The scattering peak, evident in all the intensity profiles, is consistent with the presence of a spatial correlation between micelles.

The detailed model used to fit the intensity profiles expresses the total coherent scattering intensity as a function of a scattering form factor for a micelle with a spherical core and Gaussian chains attached to the core surface and a monodisperse hard-sphere structure factor (eq A1 in Appendix). The scattering form factor consists of two self-correlation terms for the core and corona chains and two cross-correlation terms between core and corona chains as well as between different corona chains. These terms are expressed in terms of the radius of the core (R_C) and radius of gyration (R_G) of the Gaussian chains (eqs A2−A6 in Appendix).[53−58] The structure factor is described by a hard-sphere interaction model that considers short-range repulsions between hard spheres of radius (R_{hs}) (eqs A7 and A8 in Appendix). This radius should be strictly equal to half the minimum micellar center-to-center distance (ξ_S). However, Reynders and co-workers reported a decrease in hard-sphere radius with increase in concentration.[59] This is attributed to the compressibility of the corona part (PEO coronal chains in our case) of the "hard sphere". Using appropriate values for R_C, R_G, and ξ_S (the reciprocal of the peak position q^*), the intensity profiles were successfully fitted. We observed that the values of R_C (= 6 nm) and R_G (= 4.5 nm) for good fits were invariant of concentration, and the value of R_C from SANS measurements is consistent with the estimate of the size of the hydrophobic core from the cryo-SEM micrographs. The peak position for the 10 wt % solution corresponded to a micellar center-to-center distance (ξ_S) of ca. 37 nm. The term ($\xi_S - 2R_C \approx 25$ nm) represents the typical length of the PEO bridge between two micelles. This is greater than the Gaussian coil end-to-end distance (≈ 15 nm) of the 26 kg/mol PEO mid-block but considerably less than its fully stretched chain length (≈ 260 nm). This is indicative of the presence of a swollen network with moderately stretched PEO blocks. With increase in concentration, the peak position (q^*) shifts to higher values and approaches a scaling of $q^* \sim \phi^{1/3}$, indicative of an isotropic increase in micelle density (Figure 3b inset).[60] As noted above, the low-q upturn results from the presence of spatial heterogeneities arising from the clustering of micelles due to bridging interactions.[15] The heterogeneities give rise to local pockets of water, which appear as voids upon sublimation of the water in the cryo-SEM sample preparation, as discussed earlier. As concentration is increased to the point of causing soft ordering of micelles, the low-q upturn decreases and the correlation peak becomes more pronounced, as seen in the intensity profiles normalized by concentration (Figure 3b).[60]

The cryo-SEM analysis of the 10 wt % aqueous solution of FOF suggests agglomerates of flatter disklike entities, embedded in a disorganized manner in what appears to be a bicontinuous framework primarily consisting of PEO chains (Figure 2c). On increasing the concentration to 30 wt %, a bicontinuous structure (without any obvious protuberances) separating water-filled chambers with an average pore center-to-center distance of ca. 200 nm was observed. The corresponding SANS intensity profiles for solutions of FOF with polymer concentration ranging from 10 to 50 wt % are shown in Figure 4. Intensity profiles normalized by their respective concentrations are shown in Figure 4b. The high-q region, dictated by the thickness, shows good overlap, indicating its invariance to changes in concentration. The correlation peak in the mid-q region undergoes a distinct change when concentration increases above 10 wt %, which we associate the transition to the bicontinuous morphology in Figure 2d.

A form factor expression that describes scattering from randomly oriented disks of radius R_D and thickness h_D was chosen to model the high-q region for all concentrations (eqs A10 and A11 in Appendix).[61] Previous work with bicontinuous morphologies such as surfactant sponge phases has shown that the scattering profiles can be satisfactorily fitted with the form factor expression for disks, hence our choice to fit even the higher concentration profiles with the same expression.[62] All the intensity profiles were satisfactorily fitted with values of 6 nm for h_D and 5.5 nm for R_D. We emphasize that fitting the intensity profile without considering the structure factor peak would yield a slightly lower value for the disk radius though would not affect the estimate of disk thickness. However, a good fit over most of the high-q region still

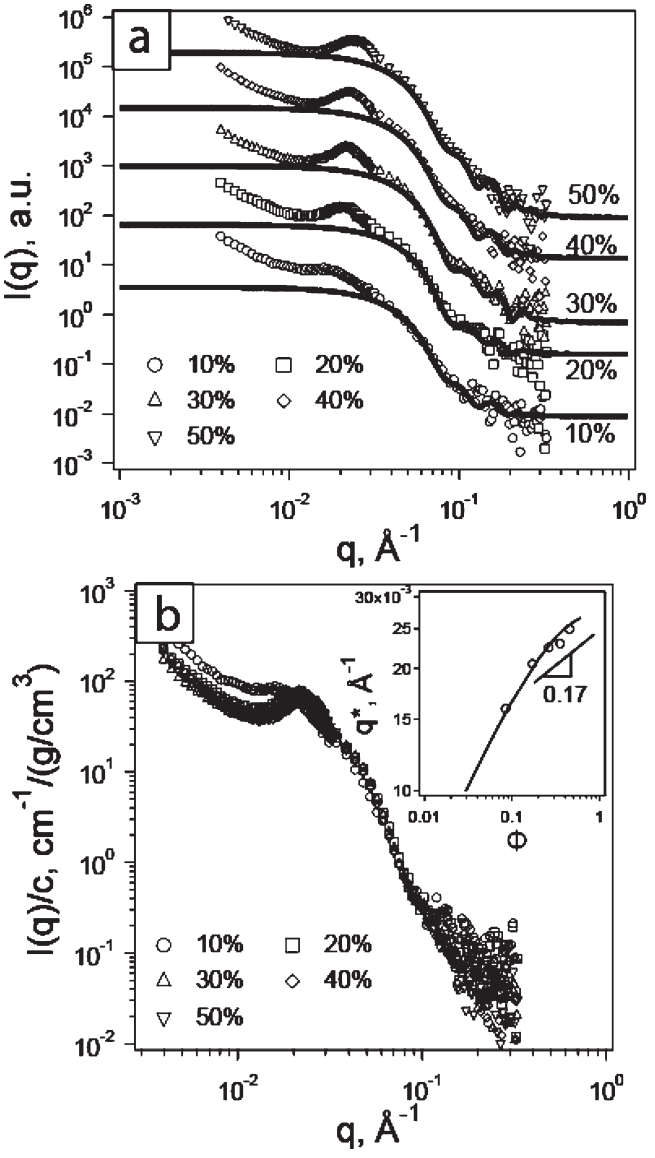

Figure 4. (a) SANS intensity profiles for FOF at different concentrations in water under PEO contrast matched conditions. For clarity, the intensity data for higher concentrations have been shifted vertically: 20% (×10), 30% (×100), 40% (×1000), and 50% (×10 000). The solid lines are fits using eqs A10 and A11. (b) Intensity normalized by concentration. Inset shows the dependence of peak position on polymer volume fraction, and the solid curve represents the fit to eq 1.

supports the disklike morphology. While the invariant fit value for h_D is anticipated from the concentration invariance of the intensity profiles in the high-q region, the constant value for R_D is less obvious and points to a need for closer examination of the bicontinuous morphology evidenced in cryo-SEM. A notable feature in all the scattering profiles is the low value of the correlation length in the bicontinuous structure, calculated from the peak position in the profiles ($\xi_D = 2\pi/q^*$). For the 30% solution, the peak position corresponds to a spacing of 28 nm, which is an order of magnitude lower than the pore size measurements from cryo-SEM micrographs. This implies that the peak results from a correlation within the walls of the bicontinuous structure that is not readily apparent in the cryo-SEM (Figure 2b). We posit a structural arrangement where the fluorocarbon disks, with PEO chains covering the surfaces, form a skeletal bicontinuous framework. The platinum coating could obscure any internal structure in the sheets in the cryo-SEM images. This morphology is reminiscent of the bicontinuous arrangement adopted by poly(*N*-isopropylacrylamide) (PNIPAM) decorated disk-shaped clay nanoparticles in microphase-separated PNIPAM/clay nanocomposite hydrogels.[63] Above the lower critical solution temperature (LCST) of PNIPAM, the polymer aggregates on the surface of the clay disk expelling water from the clay surface as the polymer−clay composite forms interpenetrating channels with water. In the case of FOF, we speculate that the extreme hydrophobicity of the PFPO core and the ensuing flat interface would force the PEO chains to stack laterally[20] and crowd the surface, forming a bicontinuous arrangement with water expelled from the PEO−PFPO interface.

Further evidence that the disklike form of the PFPO cores is retained at higher concentrations comes from the dependence of position of the correlation peak in the intensity profile on polymer concentration. With increase in concentration the peak position (q^*) shifts to higher values, approaching a scaling of $q^* \sim \phi^{0.17}$ for concentrations higher than 10 wt %. This is significantly different from the scaling relation observed for solutions of BOB. The explanation lies in the difference in the dimensionality (D) of the hydrophobic core structure; $D = 3$ for PB spheres and $D = 2$ for PFPO disks. The dependence of the correlation distance (ξ_D) on polymer volume fraction (ϕ) can be compared to an expression proposed by Torquato, Lu, and Rubinstein, describing the mean nearest-neighbor distance in a system of D-dimensional spheres ($D = 2$ for thin disks).[64]

$$\frac{\xi_D}{\sigma} = 1 + \frac{1}{2}\sqrt{\left(\frac{\pi}{a}\right)}\exp\left(\frac{b^2}{4a}\right)\operatorname{erfc}\left[\frac{b}{2\sqrt{a}}\right]$$
$$a = \frac{4\phi}{(1-\phi)^2} \qquad (1)$$
$$b = \frac{4\phi(2+\phi)}{(1-\phi)^2}$$

In this equation σ represents the minimum separation distance attainable between two adjacent disks. We found a good fit using a value of 23 nm for σ (the solid curve in the inset to Figure 4b), which is almost twice the diameter of the fluoro disk (11 nm). The difference in these two values may be attributed to the PEO chains, bridging and looping between the disks.

We have previously reported the microstructural characterization of the 10 wt % aqueous solution of BOF.[46] Cryo-SEM and contrast-matching SANS analysis supported the existence of a bicontinuous compartmentalized network in which fluorocarbon disks (ca. 14 nm in diameter and 5 nm in thickness) are distributed within thin (thickness ∼5−10 nm) PB sheets. Both faces of the sheet are covered by brushes formed by looping PEO mid-blocks, and the sheets form an open cell foamlike percolating structure with 300−700 nm pores. In this report, we examine the effect of concentration on the formation of this bicontinuous structure. Cryo-SEM analysis revealed a bicontinuous network at 30 wt % (Figure 2f), similar to that seen for 10 wt % (Figure 2e), albeit with smaller pores indicating a tighter network at higher concentrations. SANS experiments were performed under both PEO and PFPO matched conditions; the PB matched condition yields little new information distinct from the PEO matched experiment.[46] For a three-component system, the intensity profiles obtained under contrast matched conditions (where solvent cancels out the coherent contribution from one component) can be satisfactorily described with three terms: two self-scattering terms and one pairwise correlation (cross-term). The cross-correlation term can have both positive and negative contributions arising from scattering interferences from both components, thereby rendering it smaller than the two self-terms. Furthermore, if one of the two remaining components is a dominant scatterer, either

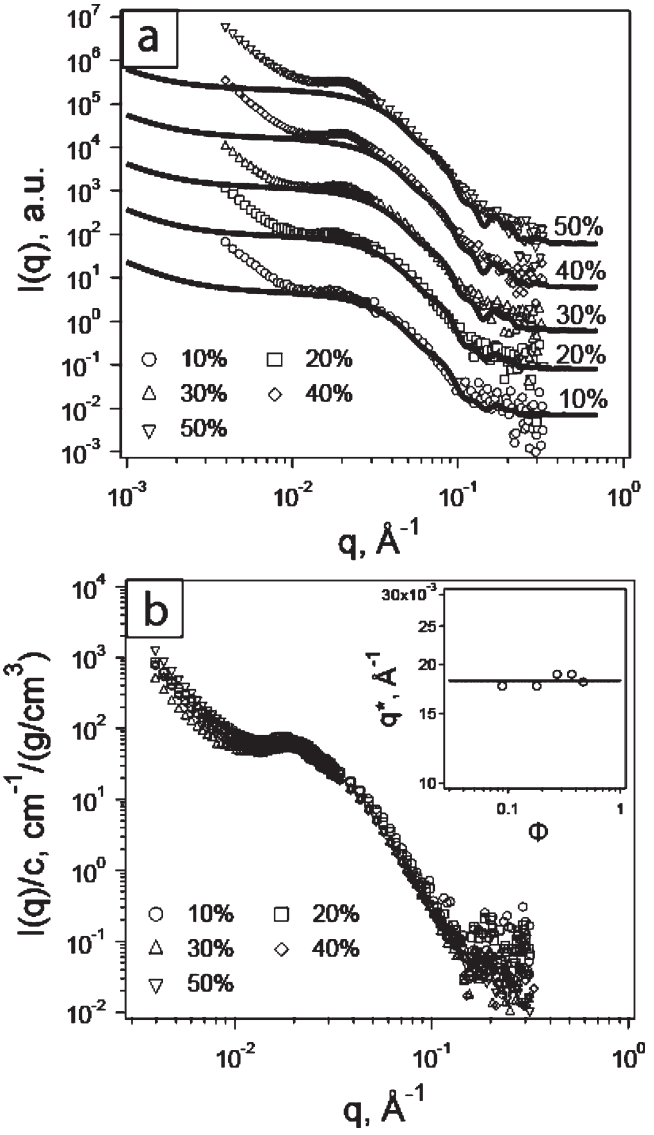

Figure 5. (a) SANS intensity profiles for BOF at different concentrations in water under PEO contrast matched condition. For clarity, the intensity data for higher concentrations have been shifted vertically: 20% (×10), 30% (×100), 40% (×1000), and 50% (×10 000). The solid lines are fits using eq A12. (b) Intensity normalized by concentration under PEO contrast matching conditions. Inset shows the independence of peak position on polymer volume fraction.

due to scattering length density or due to aggregation, the cross-contribution is further weakened. These effects allow for a reasonably good prediction of scattering profile by considering only the individual coherent contributions. Thus, the intensity profiles were fitted using a model that considers self-scattering contributions from PFPO disks, PB sheets, and PEO brushes weighted by square of their respective scattering length density differences with the solvent (see ref 46 and eq A12 in Appendix). Figure 5 shows results from PEO contrast matched solutions, in which the fluorocarbon disks are expected to dominate the scattering profile; the PFPO contrast match results are included in the Supporting Information (Figure S7). As mentioned earlier, neglecting the structure factor peak can offset the estimated value of the radius of the disk. However, a close adherence of the theoretical estimate with experimental data indicates the presence of disklike morphology. When normalized by concentration, the intensity profiles in the high-q region showed no appreciable change with increase in concentration, implying that the fluoropolymer disks do not change in shape or size, proving the resilience of the structure to changes in concentration (Figure 5b). The peak centered around 2×10^{-2} Å^{-1} was attributed to the presence of spatial correlations among the embedded fluorocarbon disks. Notably, this peak exhibits no dependence on concentration (inset in Figure 5b); this effect supports the above interpretation, since the spacing between the disks within a given sheet should be unaffected by changes in concentration. The low-q upturn in intensity results from the water-filled chambers (pores in the cryo-SEM micrographs in Figure 2e,f), which would decrease in size as concentration increases but are still larger than the length scales probed in the SANS experiment.

Discussion

The equilibrium microstructure in a two-component block copolymer (A−B) system results from the free energy balance between minimizing interfacial area and resisting any deviations of the constituent blocks from their preferred Gaussian conformations. Theoretical approaches to understanding the phase behavior of such systems identify four distinct regimes, namely "weak", "intermediate", "strong", and "superstrong" segregation.[65−67] The first two regimes are characterized by low values of the interaction parameter χ between A and B units, which results in weak perturbations of the coils from their Gaussian state. In the strong segregation regime, obtained for large enough chains and with high enough values of interfacial tension, segregation of the two blocks into their respective domains occurs with the interfacial zone between them being negligible in thickness compared to the domain dimensions. For the case of one block (A) being much smaller than the other (B), the microstructure corresponds to spherical A-rich domains (micellar cores) surrounded by matrix of B. On addition of a B-selective solvent, the system is expected to conserve this microstructure. A representative example of a block copolymer system conforming to the strong segregation regime is that of PB (A) and PEO (B).[68] Bates and co-workers have reported the existence of spherical micelles in aqueous dispersions of diblock copolymers of PB and PEO with volume fractions of PEO higher than 0.6.[69,70] One could expect that introducing a link between two diblock copolymer molecules segregated in two different micelles would bring in bridging interactions between the micelles but not affect the shape of the core. This explains the formation of networks with spherical junctions in aqueous solutions of BOB.

The superstrong segregation regime (SSSR) is obtained when the interfacial tension is so high as to overwhelm other contributions to the free energy. In this case, flat interfaces are favored as the smaller block (A) fully stretches to reduce contact with the interface. Although Semenov et al. speculated that this regime might only be experimentally accessible with ionic polymers, we have previously observed core−shell−corona disklike micelles formed from the linear terpolymer of PEO, polystyrene (PS), and fluoro-modified PB (f-PB) in water, consistent with accessing the SSSR.[71,72] We proposed that the extremely high interfacial tension between PS and f-PB was the primary reason for the formation of flat interface. The concept of superstrong segregation was then also applied to the interpretation of the multicompartment micellar morphologies formed in dilute aqueous solutions of miktoarm star terpolymers of PEO, PB, and PFPO.[21−26] Similarly, these concepts can help explain the formation of disks and sheets in aqueous dispersions of FOF and BOF. Fluorocarbons are known to bear an extremely high interfacial tension with water as compared to their hydrocarbon equivalents, and the rodlike behavior exhibited by fluorocarbon molecules in aqueous environment has been attributed to this superhydrophobicity.[73,20] Thus, the formation of a flat-interface disk-shaped assembly can be understood in aqueous dispersions of FOF. However, it has

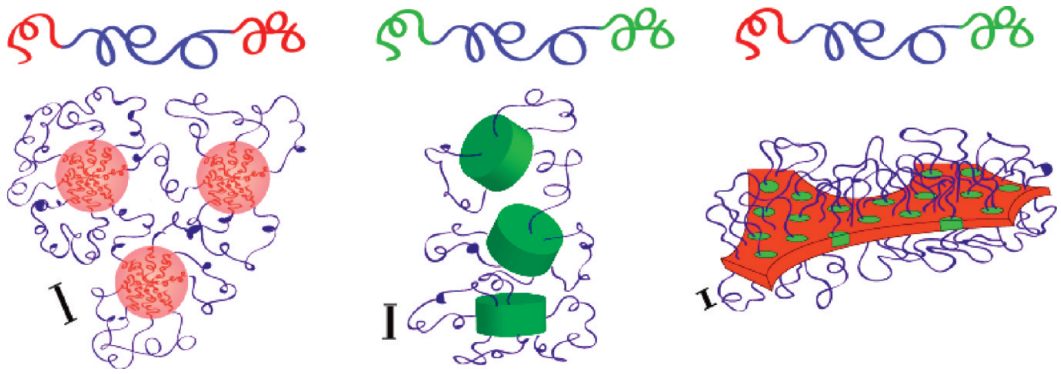

Figure 6. Schematic representations showing the dependence of network morphology on the end-groups. 1,2-Polybutadiene, poly(ethylene oxide), and poly(perfluoropropylene oxide) have been represented in red, blue, and green, respectively. The scale bars identify a length of 5 nm in each cartoon.

been argued that a solution of large isolated micellar disks is highly unstable as the hydrophobic disk edges are enthalpically unfavorable in aqueous environment.[74] In small molecule surfactants, enthalpically costly disk edges are avoided by transitioning to a bicontinuous morphology such as the sponge phase.[75] Interestingly, the aqueous systems of FOF and BOF display alternative ways of circumventing the enthalpic penalty of PFPO/water interfaces. The FOF aqueous system does so by crowding the surface of disk with PEO chains, thereby expelling water from the interface, while the BOF aqueous system associates the fluoro disks with the relatively less hydrophobic butadiene chains. While our experiments cannot distinguish between these disks being buried in the PB matrix or decorating the surface, the chain packing motif seen in multicompartment assemblies like hamburger micelles and polygonal sheets from miktoarm star terpolymers of the same component polymers that are discussed in this paper suggests that the disks are embedded in the PB matrix (as shown in Figure 6). This interplay between the two hydrophobic blocks in the BOF system gives rise to an interesting structure, contrary to a naïve expectation of spatially distinct hydrophobic domains arising from the incompatibility of the two blocks.[46]

Summary

Using a combination of cryogenic scanning electron microscopy and contrast matched small-angle neutron scattering experiments, we have investigated the dependence of morphology of a telechelic triblock polymer hydrogel on the chemical identity of the end-blocks. With similar blocks at both ends (homotelechelic), the curvature of the hydrophobic domains and hence the network morphology was driven by the interfacial tension between the hydrophobic blocks and water. The hydrophobic 1,2-polybutadiene blocks segregated into spherical domains and the presence of bridging hydrophilic mid-blocks gave rise to a three-dimensional network. Using poly(perfluoropropylene oxide) as end-blocks gave clusters of disklike micelles that arranged themselves along a bicontinuous framework at higher concentrations. For case of dissimilar end-blocks (heterotelechelic), the network morphology was influenced by the interplay between the two hydrophobic blocks such that the poly(perfluoropropylene oxide) disks preferred being embedded in a bicontinuous 1,2-polybutadiene matrix to avoid enthalpically costly interfaces of the disk edges with water. These results establish that network morphologies can be varied substantially by tuning the solvophobicity of the end-blocks and by the overall architecture (homo- vs heterotelechelic). Figure 6 provides a cartoon representation of the various proposed structures.

Acknowledgment. This work was supported by the MRSEC program of the National Science Foundation under Award DMR-0819885 at the University of Minnesota. The cryo-SEM experiments were carried out in the University of Minnesota I.T. Characterization Facility, which receives partial support from NSF through the NNIN program. We thank Dr. William F. Edmonds for providing the 1,2-polybutadiene (1.9 kg/mol) sample and Chris Frethem for help with the cryo-SEM experiments. We also acknowledge the help that we received from Dr. Steve Kline and Dr. Paul Butler with the SANS experiments. We also thank Dupont for providing the PFPO−COOH homopolymer.

Supporting Information Available: Results from nuclear magnetic resonance (NMR) spectroscopy and size exclusion chromatography (SEC) analysis of the three triblock copolymers and results from SANS experiments on PFPO matched aqueous solutions of BOF. This material is available free of charge via the Internet at http://pubs.acs.org.

Appendix. Models for Fitting SANS Intensity Profiles

a. BOB Aqueous Solutions. Details of model fitting have been explained elsewhere.[53−58] A brief overview adapted from these references follows.

The total coherent scattering intensity was given by the following expression

$$\Delta I(q) = \int D(R_C)[P_{mic}(q) + (A_{mic}(q))^2[S(q) - 1]]\, dR_C \tag{A1}$$

where $P_{mic}(q)$ is the scattering form factor for a micelle consisting of a spherical core of radius R_C and Gaussian corona chains with radius of gyration R_G attached to the core surface. There are four contributions to this term: the self-correlation of the core, the self-correlation of the corona chains, the cross-term between the sphere and the corona chains, and the cross-term between different corona chains

$$\begin{aligned} P_{mic}(q) = {} & N_{agg}{}^2\beta_{core}{}^2A_{core}{}^2(q) + N_{agg}\beta_{corona}{}^2P_{chain}(q) \\ & + 2N_{agg}{}^2\beta_{core}\beta_{corona}A_{core}(q)A_{corona}(q) \\ & + N_{agg}(N_{agg} - 1)\beta_{corona}{}^2A_{corona}{}^2(q) \end{aligned} \tag{A2}$$

Here q is the scattering wave vector, N_{agg} is the aggregation number, and β_{core} and β_{corona} are total excess scattering lengths of core and corona blocks, respectively. They are defined as $\beta_{core} = v_{core}(\rho_{core} - \rho_{solvent})$ and $\beta_{corona} = v_{corona}(\rho_{corona} - \rho_{solvent})$, where v_{core} and v_{corona} are the volumes of core and corona chains, respectively. Also, ρ_{core}, ρ_{corona}, and $\rho_{solvent}$ are the scattering length densities of core block,

corona block, and solvent, respectively. The core self-term $A_{core}^2(q)$ is given by

$$A_{core}^2(q) = \Phi^2(qR_C)\exp(-q^2\sigma_{int}^2) \quad \text{(A3)}$$

where $\Phi(x) = 3[\sin(x) - x\cos(x)]/x^3$ is the hard-sphere form factor and σ_{int} takes in account the smoothly decaying density at the surface and represents the width of interface between core and corona. The corona chain self-correlation term $P_{chain}(q)$ is given by the Debye function

$$P_{chain}(q) = \frac{2[\exp(-x) - 1 + x]}{x^2}; \quad x = q^2R_G^2 \quad \text{(A4)}$$

The form factor of corona chain features in cross-correlation terms between core and corona chains [$A_{core}(q)\ A_{corona}(q)$] and between different corona chains [$A_{corona}^2(q)$]. This is given as the normalized Fourier transform of the radial density distribution function of the corona chains ($\rho_{corona}(r)$)

$$A_{corona}(q) = \frac{4\pi\int \rho_{corona}(r)\dfrac{\sin(qr)}{qr}r^2\,dr}{4\pi\int \rho_{corona}(r)r^2\,dr}\exp(-q^2\sigma_{int}^2/2) \quad \text{(A5)}$$

A sum of two partial cubic b spline functions was chosen for $\rho_{corona}(r)$, as explained elsewhere. The form factor amplitude of the radial scattering length distribution of the micelle is given by

$$A_{mic}(q) = N_{agg}(\beta_{core}A_{core}(q) + \beta_{corona}A_{corona}(q)) \quad \text{(A6)}$$

The structure factor $S(q)$ is given in terms of Fourier transform of direct correlation function as

$$S(q) = (1 - C(q))^{-1} \quad \text{(A7)}$$

$$C(q) = -24\phi x^{-6}\big[\alpha x^3(\sin x - x\cos x) + \beta x^2(2x\sin x - (x^2-2)\cos x - 2) + 0.5\phi\alpha((4x^3 - 24x)\sin x - (x^4 - 12x^2 + 24)\cos x + 24)\big] \quad \text{(A8)}$$

where $x = q(\xi_S)$, $\alpha = (1 + 2\phi)^2(1 - \phi)^{-4}$, and $\beta = -[3\varphi(2 + \phi)^2][2(1 - \phi)^4]^{-1}$. Here φ is the hard-sphere volume fraction. The polydispersity in micelle size was accounted for, by considering a Gaussian distribution for core radii:

$$D(R_C) = \frac{1}{\sqrt{2\pi}\sigma_R}\exp\left[\frac{-(R_C - \langle R_C\rangle)^2}{2\sigma_R^2}\right]; \quad R_C > 0 \quad \text{(A9)}$$

where $\langle R_C\rangle$ is the average radius and σ_R is the width of distribution truncated at $R_C = 0$.

b. FOF Aqueous Solutions. The total coherent scattering intensity was modeled using[61]

$$\Delta I(q) = (\Delta\rho)^2 N\int_0^{\pi/2}[V_D f_D(q)]^2\sin\phi'\,d\phi' \quad \text{(A10)}$$

where $\Delta\rho$ represents the difference in the scattering length densities of disk core block (PFPO) and solvent (PEO contrast matched), respectively. N and V_D represent the number of disks in the solution and the volume of each disk, respectively. The disk form factor ($f_D^2(q)$) is averaged over all orientations by integrating over ϕ', where ϕ' is the angle between the scattering vector q and the normal to the face of the disk.

$$\langle f_D^2(q)\rangle_{\phi'} = \int_0^{\pi/2}\left[\left(\frac{\sin\left(\frac{qh_D}{2}\cos\phi'\right)}{\frac{qh_D}{2}\cos\phi'}\right)\left(\frac{2J_1(qR_D\sin\phi')}{qR_D\sin\phi'}\right)\right]^2 \sin\phi'\,d\phi' \quad \text{(A11)}$$

Here R_D and h_D represent the radius and thickness of the disk, respectively.

c. Aqueous Solutions of BOF. The model fitting has been explained elsewhere.[46] A brief overview follows.

$$\begin{aligned}\Delta I(q) = {} & (\Delta\rho^*)^2|_{PFPO}\{N\int_0^{\pi/2}[V_D f_D(q)]^2\sin\phi'\,d\phi'\} \\ & + (\Delta\rho^*)^2|_{PB}\left\{\frac{4\pi f_{PB}\phi_{polymer}}{dq^4}\left[1 - \cos(qd)\exp\left(\frac{-q^2\sigma_d^2}{2}\right)\right]\right\} \\ & + (\Delta\rho^*)^2|_{PEO}\left\{\frac{(\psi_{PEO})^2 f_{PEO}\phi_{polymer}}{q^2}\right[2(L + d/2) \\ & \frac{\sin[q(L + d/2)]}{q(L + d/2)}\exp\left(\frac{-q^2\sigma_L^2}{2}\right) \\ & - d\frac{\sin[q(d/2)]}{q(d/2)}\exp\left(\frac{-q^2\sigma_d^2}{2}\right)\Big]^2 \\ & + \phi_{polymer}f_{PEO}\psi_{PEO}\xi_b^3(1/\mu)\frac{\sin(\mu\arctan(q\xi_b))}{q\xi_b(1 + (q\xi_b)^2)^{\mu/2}}\Big\}\end{aligned} \quad \text{(A12)}$$

Here ($\Delta\rho^*$) represents the difference between the scattering length density of polymer and solvent. The volume fractions of each block in the copolymer and of the polymer in the solution are represented by f and $\phi_{polymer}$, respectively. The first term in the equation represents the form factor for the disk-shaped fluoro domains. The disk form factor ($f_D^2(q)$) is given in eq A11. The second term, weighted by the scattering length density of PB, corresponds to the form factor of the PB sheets of thickness d. The last two terms, weighted by the scattering length density of PEO, include the form factor for the PEO brushes of length L and blob scattering from the PEO chains, respectively. ψ_{PEO} represents the volume fraction of PEO in the brush layer diluted by solvent. The blob size (ξ_b), which determines PEO brush length (L), was estimated using approach followed elsewhere. The term μ is related to the Flory exponent (υ) by $\mu = 1/\upsilon - 1$, and for PEO in water ($\upsilon = 0.66$), $\mu = 0.515$.

References and Notes

(1) Altinok, H.; Yu, G.-E.; Nixon, S. K.; Gorry, P. A.; Attwood, D.; Booth, C. *Langmuir* **1997**, *13*, 5837–5848.
(2) Xu, B.; Li, L.; Yekta, A.; Masoumi, Z.; Kanagalingam, S.; Winnik, M. A.; Zhang, K.; Macdonald, P. M.; Menchen, S. *Langmuir* **1997**, *13*, 2447–2456.
(3) Kelarakis, A.; Yuan, X.-F.; Mai, S.-M.; Yang, Y.-W.; Booth, C. *Phys. Chem. Chem. Phys.* **2003**, *5*, 2628–2634.

(4) Kelarakis, A.; Havredaki, V.; Yuan, X.-F.; Chaibundit, C.; Booth, C. *Macromol. Chem. Phys.* **2006**, *207*, 903–909.
(5) Raspaud, E.; Lairez, D.; Adam, M.; Carton, J. P. *Macromolecules* **1994**, *27*, 2956–64.
(6) Lairez, D.; Adam, M.; Carton, J. P.; Raspaud, E. *Macromolecules* **1997**, *30*, 6798–6809.
(7) Balsara, N. P.; Tirrell, M.; Lodge, T. P. *Macromolecules* **1991**, *24*, 1975–86.
(8) Berret, J.-F.; Calvet, D.; Collet, A.; Viguier, M. *Curr. Opin. Colloid Interface Sci.* **2003**, *8*, 296–306.
(9) Zhou, Z.; Chu, B.; Nace, V. M.; Yang, Y.-W.; Booth, C. *Macromolecules* **1996**, *29*, 3663–4.
(10) Zhou, Z.; Yang, Y.-W.; Booth, C.; Chu, B. *Macromolecules* **1996**, *29*, 8357–8361.
(11) Liu, T.; Zhou, Z.; Wu, C.; Nace, V. M.; Chu, B. *J. Phys. Chem. B* **1998**, *102*, 2875–2882.
(12) Zhou, Z.; Chu, B. *Macromolecules* **1994**, *27*, 2025–33.
(13) Mai, S.-M.; Ludhera, S.; Heatley, F.; Attwood, D.; Booth, C. *J. Chem. Soc., Faraday Trans.* **1998**, *94*, 567–572.
(14) Liu, T.; Zhou, Z.; Wu, C.; Chu, B.; Schneider, D. K.; Nace, V. M. *J. Phys. Chem. B* **1997**, *101*, 8808–8815.
(15) Mortensen, K.; Brown, W.; Jørgensen, E. *Macromolecules* **1994**, *27*, 5654–66.
(16) Yang, Y.-W.; Ali-Adib, Z.; McKeown, N. B.; Ryan, A. J.; Attwood, D.; Booth, C. *Langmuir* **1997**, *13*, 1860–1861.
(17) Ricardo, N. M. P. S.; Honorato, S. B.; Yang, Z.; Castelletto, V.; Hamley, I. W.; Yuan, X.-F.; Attwood, D.; Booth, C. *Langmuir* **2004**, *20*, 4272–4278.
(18) Agrawal, S. K.; Sanabria-DeLong, N.; Tew, G. N.; Bhatia, S. R. *Macromolecules* **2008**, *41*, 1774–1784.
(19) Tae, G.; Kornfield, J. A.; Hubbell, J. A.; Lal, J. *Macromolecules* **2002**, *35*, 4448–4457.
(20) Tae, G.; Kornfield, J. A.; Hubbell, J. A.; Johannsmann, D.; Hogen-Esch, T. E. *Macromolecules* **2001**, *34*, 6409–6419.
(21) Li, Z.; Kesselman, E.; Talmon, Y.; Hillmyer, M. A.; Lodge, T. P. *Science* **2004**, *306*, 98–101.
(22) Lodge, T. P.; Bang, J.; Li, Z.; Hillmyer, M. A.; Talmon, Y. *Faraday Discuss.* **2004**, *128*, 1–12.
(23) Lodge, T. P.; Rasdal, A.; Li, Z.; Hillmyer, M. A. *J. Am. Chem. Soc.* **2005**, *127*, 17608–17609.
(24) Li, Z.; Hillmyer, M. A.; Lodge, T. P. *Nano Lett.* **2006**, *6*, 1245–1249.
(25) Li, Z.; Hillmyer, M. A.; Lodge, T. P. *Langmuir* **2006**, *22*, 9409–9417.
(26) Li, Z.; Hillmyer, M. A.; Lodge, T. P. *Macromolecules* **2006**, *39*, 765–771.
(27) Saito, N.; Liu, C.; Lodge, T. P.; Hillmyer, M. A. *Macromolecules* **2008**, *41*, 8815–8822.
(28) Liu, C.; Hillmyer, M. A.; Lodge, T. P. *Langmuir* **2008**, *24*, 12001–12009.
(29) Liu, C.; Hillmyer, M. A.; Lodge, T. P. *Langmuir* **2009**, *25*, 13718–13725.
(30) Staehler, K.; Selb, J.; Candau, F. *Langmuir* **1999**, *15*, 7565–7576.
(31) Staehler, K.; Selb, J.; Barthelemy, P.; Pucci, B.; Candau, F. *Langmuir* **1998**, *14*, 4765–4775.
(32) Kotzev, A.; Laschewsky, A.; Adriaensens, P.; Gelan, J. *Macromolecules* **2002**, *35*, 1091–1101.
(33) Pochan, D. J.; Chen, Z.; Cui, H.; Hales, K.; Qi, K.; Wooley, K. L. *Science* **2004**, *306*, 94–97.
(34) Kubowicz, S.; Thunemann Andreas, F.; Weberskirch, R.; Mohwald, H. *Langmuir* **2005**, *21*, 7214–9.
(35) Kubowicz, S.; Baussard, J.-F.; Lutz, J.-F.; Thuenemann, A. F.; von Berlepsch, H.; Laschewsky, A. *Angew. Chem., Int. Ed.* **2005**, *44*, 5262–5265.
(36) Duxin, N.; Liu, F.; Vali, H.; Eisenberg, A. *J. Am. Chem. Soc.* **2005**, *127*, 10063–10069.
(37) Zhu, J.; Jiang, W. *Macromolecules* **2005**, *38*, 9315–9323.
(38) Thuenemann, A. F.; Kubowicz, S.; Von Berlepsch, H.; Moehwald, H. *Langmuir* **2006**, *22*, 2506–2510.
(39) Cui, H.; Chen, Z.; Zhong, S.; Wooley, K. L.; Pochan, D. J. *Science* **2007**, *317*, 647–650.
(40) Mao, J.; Ni, P.; Mai, Y.; Yan, D. *Langmuir* **2007**, *23*, 5127–5134.
(41) Fustin, C.-A.; Abetz, V.; Gohy, J.-F. *Eur. Phys. J. E* **2005**, *16*, 291–302.
(42) Hadjichristidis, N.; Iatrou, H.; Pitsikalis, M.; Pispas, S.; Avgeropoulos, A. *Prog. Polym. Sci.* **2005**, *30*, 725–782.
(43) Weberskirch, R.; Preuschen, J.; Spiess, H. W.; Nuyken, O. *Macromol. Chem. Phys.* **2000**, *201*, 995–1007.
(44) Shunmugam, R.; Smith, C. E.; Tew, G. N. *J. Polym. Sci., Polym. Chem.* **2007**, *45*, 2601–2608.
(45) Shen, W.; Zhang, K.; Kornfield, J. A.; Tirrell, D. A. *Nature Mater.* **2006**, *5*, 153–158.
(46) Taribagil, R. R.; Hillmyer, M. A.; Lodge, T. P. *Macromolecules* **2009**, *42*, 1796–1800.
(47) Hillmyer, M. A.; Bates, F. S. *Macromolecules* **1996**, *29*, 6994–7002.
(48) Chen, J.; Frisbie, C. D.; Bates, F. S. *J. Phys. Chem. C* **2009**, *113*, 3903–3908.
(49) Jain, S.; Dyrdahl, M. H. E.; Gong, X.; Scriven, L. E.; Bates, F. S. *Macromolecules* **2008**, *41*, 3305–3316.
(50) Glinka, C. J.; Barker, J. G.; Hammouda, B.; Krueger, S.; Moyer, J. J.; Orts, W. J. *J. Appl. Crystallogr.* **1998**, *31*, 430–445.
(51) Beaudoin, E.; Borisov, O.; Lapp, A.; Billon, L.; Hiorns, R. C.; François, J. *Macromolecules* **2002**, *35*, 7436–7447.
(52) Kline, S. R. *J. Appl. Crystallogr.* **2006**, *39*, 895–900.
(53) Castelletto, V.; Hamley, I. W.; Pedersen, J. S. *J. Chem. Phys.* **2002**, *117*, 8124–8129.
(54) Castelletto, V.; Hamley, I. W.; Pedersen, J. S. *Langmuir* **2004**, *20*, 2992–2994.
(55) Pedersen, J. S.; Svaneborg, C.; Almdal, K.; Hamley, I. W.; Young, R. N. *Macromolecules* **2003**, *36*, 416–433.
(56) Pedersen, J. S. *J. Appl. Crystallogr.* **1998**, *31*, 488–489.
(57) Pedersen, J. S.; Hamley, I. W.; Ryu, C. Y.; Lodge, T. P. *Macromolecules* **2000**, *33*, 542–550.
(58) Pedersen, J. S.; Gerstenberg, M. C. *Macromolecules* **1996**, *29*, 1363–1365.
(59) Reynders, K.; Mischenko, N.; Kleppinger, R.; Reynaers, H.; Koch, M. H.; Mortensen, K. *J. Appl. Crystallogr.* **1997**, *30*, 684–689.
(60) Beaudoin, E.; Borisov, O.; Lapp, A.; Billon, L.; Hiorns, R. C.; François, J. *Macromolecules* **2002**, *35*, 7436–7447.
(61) Guinier, A.; Fournet, G. *Small-Angle Scattering of X-rays*; John Wiley and Sons: New York, 1955.
(62) Lei, N.; Safinya, C. R.; Roux, D.; Liang, K. S. *Phys. Rev. E: Stat. Phys., Plasmas, Fluids, Relat. Interdiscip. Top.* **1997**, *56*, 608–613.
(63) Osaka, N.; Endo, H.; Nishida, T.; Suzuki, T.; Li, H.-j.; Haraguchi, K.; Shibayama, M. *Phys. Rev. E: Stat., Nonlinear, Soft Matter Phys.* **2009**, *79*, 060801/1–060801/4.
(64) Torquato, S.; Lu, B.; Rubinstein, J. *Phys. Rev. A* **1990**, *41*, 2059–75.
(65) Matsen, M. W.; Bates, F. S. *Macromolecules* **1996**, *29*, 1091–8.
(66) Nyrkova, I. A.; Khokhlov, A. R.; Doi, M. *Macromolecules* **1993**, *26*, 3601–10.
(67) Semenov, A. N.; Nyrkova, I. A.; Khokhlov, A. R. *Macromolecules* **1995**, *28*, 7491–500.
(68) Jain, S. Ph.D. Dissertation, University of Minnesota, Minneapolis, MN, **2005**.
(69) Won, Y.-Y.; Brannan, A. K.; Davis, H. T.; Bates, F. S. *J. Phys. Chem. B* **2002**, *106*, 3354–3364.
(70) Jain, S.; Dyrdahl, M. H. E.; Gong, X.; Scriven, L. E.; Bates, F. S. *Macromolecules* **2008**, *41*, 3305–3316.
(71) Lodge, T. P.; Hillmyer, M. A.; Zhou, Z.; Talmon, Y. *Macromolecules* **2004**, *37*, 6680–6682.
(72) Zhou, Z.; Li, Z.; Ren, Y.; Hillmyer, M. A.; Lodge, T. P. *J. Am. Chem. Soc.* **2003**, *125*, 10182–10183.
(73) Kashimoto, K.; Yoon, J.; Hou, B.; Chen, C.-h.; Lin, B.; Aratono, M.; Takiue, T.; Schlossman, M. L. *Phys. Rev. Lett.* **2008**, *101*, 076102/1–076102/4.
(74) Ben-Shaul, A.; Szleifer, I.; Gelbart, W. M. *J. Chem. Phys.* **1985**, *83*, 3597–611.
(75) Roux, D.; Coulon, C.; Cates, M. E. *J. Phys. Chem.* **1992**, *96*, 4174–87.